Dedicated to Professor Iwo Białynicki-Birula on His 90th Birthday

— ◇ —

Vortex Structures and Momentum Sharing in Dynamic Sauter–Schwinger Process

A. Bechler*, F. Cajiao Vélez, K. Krajewska and J.Z. Kamiński

Institute of Theoretical Physics, Faculty of Physics, University of Warsaw, Pasteura 5, 02-093 Warszawa, Poland

Published: 14.06.2023

Doi: 10.12693/APhysPolA.143.S18 *e-mail: adam.bechler@fuw.edu.pl

Vortex pattern formation in the electron–positron pair creation from a vacuum by a time-dependent electric field of linear polarization is analyzed. It is demonstrated that in such a scenario the momentum distributions of the created particles exhibit vortex–antivortex pairs. Their sensitivity to the laser field parameters, such as field frequency and intensity, is also studied. Specifically, it is shown that with increasing field frequency across a threshold, additional vortex–antivortex pairs appear. Their location in the momentum space is consistent with the general threshold behavior of the probability distributions of the created electrons (positrons). Namely, while for small field frequencies the particles tend to be created along the field polarization direction, for large enough frequencies, they are predominantly generated in the perpendicular direction. Such a change in the longitudinal and transverse momentum sharing of the created particles occurs across a threshold.

topics: electron–positron pair creation, vortices, threshold effects, Dirac–Heisenberg–Wigner formalism

1. Introduction

The nonlinear response of the quantum vacuum to macroscopic electromagnetic fields, leading to the creation of electron–positron (e^-e^+) pairs, has been predicted by Sauter [1], Heisenberg and Euler [2], and Schwinger [3]. Since then, various authors have made significant contributions to our current understanding of this process, which we will refer to as the Sauter–Schwinger process. Specifically, Białynicki-Birula, Górnicki and Rafelski have established a new framework for treating the quantum vacuum in electromagnetic fields [4] (see also [5, 6] and the Ph.D. thesis of Ł. Rudnicki [7]). This is by means of what they called the Dirac–Heisenberg–Wigner (DHW) function, which describes the e^-e^+ densities in phase space. Later on, the method was largely explored for the case of spatially homogeneous electric fields (see, e.g., [8–16]). For instance, the quantum kinetic approach was recovered in that case [8] and various analytical results for exactly solvable fields were derived [8–10]. Recently, the spontaneous formation of time-crystal structures in the e^-e^+ pair creation was discovered by Białynicki-Birula and Białynicka-Birula in [16]. Other applications of the DHW formalism in the context of pair creation concern the case of parallel spatially homogeneous electric and magnetic fields [17], the standing electric wave [18–21], and inhomogeneous electric and magnetic fields in one spatial direction [22–24]. The latter limitation follows entirely from the performing capabilities of current computers, as the DHW method is very general and can be used in arbitrary dimensions. It is also important to emphasize that the DHW method is not limited to describing pair creation from a vacuum. For instance, it was argued that DHW is very useful for practical plasma applications such as studies of Langmuir waves in high-density plasma [25].

Another area of research to which Professor I. Białynicki-Birula contributed largely is related to quantum vortices. It follows from the hydrodynamical formulation of quantum mechanics that a probability fluid can inherently possess vortices [26]. They are defined as phase singularities of the wave function and their strength is measured in terms

of the topological charge [26–28]. As was discussed in [27, 28], vortices form isolated lines that either emerge from a single point forming a closed loop, or can be created as a pair of lines with opposite topological charges. These mechanisms of creation and subsequent annihilation of vortex–antivortex pairs were confirmed recently in a series of papers focused on vortex structures in strong-field ionization [29–33]. Specifically, it was demonstrated that vortex structures are very sensitive to the laser field parameters, so they can be easily steered by the field. While the aforementioned papers deal with quantum vortices in nonrelativistic quantum mechanics, their notion can also be extended to relativistic quantum theory, as proposed by Białynicki-Birula and Białynicka-Birula in [34]. See also, the construction of knotted vortex states, or hopfion-like states in relativistic quantum mechanics [35] by the same authors.

Note that the creation and ionization of an electron–positron pair are formally similar since they are both threshold-related phenomena that can be driven by external dynamically changing fields. For this reason, one might expect similar effects to be exhibited in both processes. Keeping this in mind, in the current paper we investigate whether vortex structures similar to [29–33] can be observed in the probability amplitude of e^-e^+ pair creation in the presence of a linearly polarized time-dependent electric field. Our emphasis will be on the threshold behavior of those patterns, which can be studied, for instance, by changing the frequency of the driving field. As we will show, this is in agreement with the longitudinal and transverse momentum sharing of the created particles across the threshold, which has been studied in [36]. At this point, we would like to mention that other structures, known as spiral vortex patterns, were found in strong-field ionization [37, 38] and later in pair production [14, 15] for certain combinations of circularly polarized electric field pulses. However, as demonstrated in [31], in the case of ionization such spirals in the momentum distributions of photoelectrons do not necessarily carry a nonzero topological charge, which distinguishes them from vortices analyzed in [29–33]. The same is expected to hold for pair creation.

Our paper is organized as follows. Based on the original derivation presented in [4], we introduce the DHW formalism in Sect. 2. The bispinorial decomposition of the DHW-function for a spatially homogeneous electric field is presented in Sect. 3, and the final equations for a linear polarization are given in Sect. 4. Section 5 is devoted to the vortex patterns in the creation of e^-e^+ pairs and their sensitivity to external field parameters, especially when passing across a threshold. Another threshold-related effect is discussed in Sect. 6, where we demonstrate how particle momentum is redistributed across the threshold of pair creation. Our final remarks are given in Sect. 7.

2. The DHW-function for fermion field

The DHW-function for the fermion field is defined as [4]

$$W_{\alpha\beta}(\boldsymbol{x},\boldsymbol{p},t)=-\frac{1}{2}\int \mathrm{d}^3s\,\mathrm{e}^{-\mathrm{i}\boldsymbol{p}\cdot\boldsymbol{s}}\left\langle 0\right|\mathcal{U}(\boldsymbol{s},\boldsymbol{x},t)\left[\Psi_\alpha(\boldsymbol{x}+\boldsymbol{s}/2,t),\,\Psi^\dagger_\beta(\boldsymbol{x}-\boldsymbol{s}/2,t)\right]\left|0\right\rangle, \tag{1}$$

where the factor $\mathcal{U}(\boldsymbol{s},\boldsymbol{x},t)$ contains line integral of the vector potential in temporal gauge $A^0=0$,

$$\mathcal{U}(\boldsymbol{s},\boldsymbol{x},t)=\exp\left[-\mathrm{i}e\int\limits_{-1/2}^{1/2}\mathrm{d}\xi\;\boldsymbol{s}\cdot\boldsymbol{A}\big(\boldsymbol{x}+\xi\boldsymbol{s},t\big)\right], \tag{2}$$

and assures gauge invariance of the DHW-function, whereas Ψ_α, Ψ_β are the fermion field operators in the Heisenberg picture. We use here the version of the DHW-function with the vacuum expectation value [8]; in general, however, any pure or mixed state can be used [4]. The DHW-function is a 4×4 Hermitian matrix and as such can be decomposed in terms of 16 Hermitian matrices Γ_a with real coefficients depending generally on $\boldsymbol{x}$, $\boldsymbol{p}$ and time t. Matrices Γ_a $(a=0,1,2,\ldots,15)$ can be constructed as Kronecker products of two sets of Pauli matrices (including the identity matrix), (I_2,ρ_j) and (I_2,σ_j) [4]. The correspondence is as follows

$$\begin{aligned}
&\Gamma_0=I_4, && \Gamma_j=\rho_j\otimes I_2,\\
&\Gamma_{j+3}=I_2\otimes\sigma_j, && \Gamma_{j+6}=\rho_1\otimes\sigma_j,\\
&\Gamma_{j+9}=\rho_2\otimes\sigma_j, && \Gamma_{j+12}=\rho_3\otimes\sigma_j,
\end{aligned} \tag{3}$$

where index $j=1,2,3$. In terms of standard γ-matrices,

$$\begin{aligned}
&\Gamma_0=I_4, && \Gamma_1=\gamma_5, && \Gamma_2=-\mathrm{i}\gamma^0\gamma_5,\\
&\Gamma_3=\gamma^0, && \Gamma_{j+3}=\Sigma^j, && \Gamma_{j+6}=\alpha^j,\\
&\Gamma_{j+9}=-\mathrm{i}\gamma^j, && \Gamma_{j+12}=\gamma^0\Sigma^j,
\end{aligned} \tag{4}$$

where $\gamma_5=\mathrm{i}\gamma^0\gamma^1\gamma^2\gamma^3$, and $\Sigma^j=\gamma^5\alpha^j$ are the 4×4 spin matrices. With the use of (4) expansion of the DHW-function can be written in the form [4]

$$\begin{aligned}
W(\boldsymbol{x},\boldsymbol{p},t)=\frac{1}{4}\big(&f_0+\gamma_5 f_1-\mathrm{i}\gamma^0\gamma_5 f_2+\gamma^0 f_3\\
&+\boldsymbol{\Sigma}\cdot\boldsymbol{g}_0+\boldsymbol{\alpha}\cdot\boldsymbol{g}_1-\mathrm{i}\boldsymbol{\gamma}\cdot\boldsymbol{g}_2+\gamma^0\boldsymbol{\Sigma}\cdot\boldsymbol{g}_3\big).
\end{aligned} \tag{5}$$

The dimensionless expansion coefficients are the same as f_0, f_1, f_2, f_3 and $\boldsymbol{g}_0$, $\boldsymbol{g}_1$, $\boldsymbol{g}_2$, $\boldsymbol{g}_3$ used in [4].

The equations fulfilled by the expansion coefficients can be found by calculating their time derivatives using the Dirac equation for the fermion field operators. In deriving these equations one usually adopts the Hartree-, or mean electromagnetic field-approximation, neglecting its quantum fluctuations [4, 8]. This is equivalent to the replacements $\langle 0|\,\hat{F}^{\mu\nu}(\boldsymbol{x},t)\mathcal{U}(\boldsymbol{s},\boldsymbol{x},t)\big[\,\Psi(\boldsymbol{x}_1,t),\,\Psi^\dagger(\boldsymbol{x}_2,t)\big]\,|0\rangle \;\to\; F^{\mu\nu}(\boldsymbol{x},t)\,\big\langle 0\big|\,\mathcal{U}(\boldsymbol{s},\boldsymbol{x},t)\big[\,\Psi(\boldsymbol{x}_1,t),\,\Psi^\dagger(\boldsymbol{x}_2,t)\big]\,\big|0\big\rangle$, i.e., the operator of the quantum electromagnetic field is replaced by classical C-number field. The application of the Dirac equation for the fermion field operators in the general case of the space- and time-dependent electromagnetic field results in a complicated system of 16 integro-differential equations for the expansion coefficients of the DHW-function. These equations significantly simplify in the case of a spatially homogeneous electric field, which is the subject of main interest in the present paper. The initial conditions are determined by the free vacuum value of the DHW-function. It follows then from (1) with zero electromagnetic field and free Dirac field operators that only the coefficients f_3 and $\boldsymbol{g}_1$ survive, and their vacuum values are

$$f_3^{\rm vac} = -\frac{2mc^2}{E_{\boldsymbol{p}}}, \quad \boldsymbol{g}_1^{\rm vac} = -\frac{2c\,\boldsymbol{p}}{E_{\boldsymbol{p}}}, \tag{6}$$

where $E_{\boldsymbol{p}} = \sqrt{c^2\boldsymbol{p}^2 + m^2c^4}$ is the free particle energy. In the case of a spatially homogeneous electric field, only the coefficients $\boldsymbol{g}_0$ and $\boldsymbol{g}_2$ couple to the vacuum values (6), so that it is sufficient to consider the 10 equations for f_3, $\boldsymbol{g}_0$, $\boldsymbol{g}_1$, $\boldsymbol{g}_2$. They have the form [9, 10]

$$\Big(\partial_t + e\,\boldsymbol{\mathcal{E}}(t)\cdot\nabla_{\boldsymbol{p}}\Big)\,W(\boldsymbol{p},t) = \frac{c}{\hbar}\,M(\boldsymbol{p})W(\boldsymbol{p},t), \tag{7}$$

where W denotes the 10-dimensional vector

$$W = [f_3,\,\boldsymbol{g}_0,\,\boldsymbol{g}_1,\,\boldsymbol{g}_2], \tag{8}$$

and the 10×10 matrix M has the following block structure

$$M(\boldsymbol{p}) = \begin{bmatrix} 0 & \boldsymbol{0}^T & \boldsymbol{0}^T & 2\boldsymbol{p}^T \\ \boldsymbol{0} & \mathbb{O}_3 & 2\boldsymbol{p}\times & \mathbb{O}_3 \\ \boldsymbol{0} & 2\boldsymbol{p}\times & \mathbb{O}_3 & -2mc\,I_3 \\ -2\boldsymbol{p} & \mathbb{O}_3 & 2mc\,I_3 & \mathbb{O}_3 \end{bmatrix}, \tag{9}$$

where $\boldsymbol{0}$ and $\boldsymbol{p}$ are the 3-dimensional null and momentum column vectors, $\mathbb{O}_3$ — 3×3 null matrix, and I_3 is the 3-dimensional identity matrix. The notation $\boldsymbol{p}\times$ means that when acting on the 3-dimensional vector to the right, it gives its vector product with $\boldsymbol{p}$. Explicitly,

$$\boldsymbol{p}\times = \begin{bmatrix} 0 & -p_3 & p_2 \\ p_3 & 0 & -p_1 \\ -p_2 & p_1 & 0 \end{bmatrix}. \tag{10}$$

In closing this section, we note that the physical interpretation of the DHW-functions can be found in [4]. In particular, the phase space energy density is given by [4, 11],

$$\varepsilon(t,\boldsymbol{r},\boldsymbol{p}) = c\,\boldsymbol{p}\cdot\boldsymbol{g}_1(t,\boldsymbol{r},\boldsymbol{p}) + mc^2 f_3(t,\boldsymbol{r},\boldsymbol{p}). \tag{11}$$

The one particle distribution function, which will be used in Sect. 5 for numerical analysis of momentum distributions, is defined as [11]

$$f(t,\boldsymbol{r},\boldsymbol{p}) = \frac{\varepsilon(t,\boldsymbol{r},\boldsymbol{p}) - \varepsilon_{\rm vac}}{2E_{\boldsymbol{p}}} = \frac{\varepsilon(t,\boldsymbol{r},\boldsymbol{p})}{2E_{\boldsymbol{p}}} + 1, \tag{12}$$

where $\varepsilon_{\rm vac}$ was expressed by vacuum DHW-functions (6). It is also worth noting that the DHW formalism is very general, as it allows one to account for an arbitrary electromagnetic field. However, for a spatially homogeneous electric field, other approaches can be conveniently applied; one of which is developed next.

3. Bispinorial representation of the DHW-functions for spatially homogeneous electric field

We consider the Dirac equation in the spatially homogeneous electric field $\boldsymbol{\mathcal{E}}(t) = -\partial_t\boldsymbol{\mathcal{A}}(t)$, with the vector potential vanishing both for $t\to-\infty$ and $t\to\infty$. Due to the translational invariance of the problem, the spatial dependence of the wave function is of the plane wave type,

$$\Psi(t,\boldsymbol{x}) = \exp\left(\frac{\rm i}{\hbar}\boldsymbol{p}\cdot\boldsymbol{x}\right)\,\Phi_{\boldsymbol{p}\,r}(t), \tag{13}$$

where the time-dependent bispinor $\Phi_{\boldsymbol{p}\,r}(t)$ is labeled by the asymptotic momentum $\boldsymbol{p}$ and the spin index r. It fulfills the equation

$${\rm i}\hbar\,\partial_t\,\Phi_{\boldsymbol{p}r}(t) = H_{\rm D}(t)\;\Phi_{\boldsymbol{p}\,r}(t), \tag{14}$$

where the time-dependent Hamiltonian reads

$$H_{\rm D}(t) = c\,\boldsymbol{\alpha}\cdot\big(\boldsymbol{p} - e\,\boldsymbol{\mathcal{A}}(t)\big) + \gamma^0 mc^2. \tag{15}$$

To make contact with the DHW-functions, we construct 16 expressions bilinear in the bispinor $\Phi_{\boldsymbol{p}r}(t)$

$$S_a(\boldsymbol{p},t) = \sum_r \Phi^\dagger_{\boldsymbol{p}r}(t)\Gamma_a\,\Phi_{\boldsymbol{p}r}(t). \tag{16}$$

Using the Dirac equation (14) and its Hermitian conjugate, one finds equations fulfilled by the functions S_a,

$$\partial_t S_a = \frac{\rm i}{\hbar}\sum_r \Phi^\dagger_{\boldsymbol{p}r}\big[\;H_{\rm D}(t),\;\Gamma_a\;\big]\;\Phi_{\boldsymbol{p}r}. \tag{17}$$

The Dirac Hamiltonian $H_{\rm D}(t)$ can be written in terms of the Γ-matrices as

$$H_{\rm D}(t) = c\,\Gamma_{j+6}\big(p^j - e\mathcal{A}^j(t)\big) + mc^2\Gamma_3, \tag{18}$$

where the summation convention for the Cartesian index j is used. The Γ matrices fulfill commutation relations

$$[\Gamma_a,\,\Gamma_b] = {\rm i}\sum_{c=0}^{15} f^c_{ab}\,\Gamma_c, \tag{19}$$

where f^c_{ab} are the real structure constants of the algebra of Γ matrices. Substituting (18) into (17) and using (19) gives

$$\partial_t S_a = -\frac{c}{\hbar}(p^j - e\mathcal{A}^j)\sum_{b=0}^{15} f^b_{j+6,a}S_b - \frac{mc^2}{\hbar}\sum_{b=0}^{15} f^b_{3a}\,S_b. \tag{20}$$

The nonvanishing structure constants are (indices i, j, k take the values $1, 2, 3$)

$$
\begin{aligned}
&f^{k}_{ij} = 2\epsilon_{ijk},\\
&f^{i+12}_{1,i+9} = 2, \quad f^{i+9}_{1,i+12} = -2, \quad f^{i+12}_{2,i+6} = -2,\\
&f^{i+6}_{2,i+12} = 2, \quad f^{i+9}_{3,i+6} = 2, \quad f^{i+6}_{3,i+9} = -2,\\
&f^{k+3}_{i+3,j+3}{=}f^{k+3}_{i+6,j+6} = f^{k+3}_{i+9,j+9} = f^{k+3}_{i+12,j+12}{=}2\epsilon_{ijk},\\
&f^{k+6}_{i+3,j+6}{=}f^{k+9}_{i+3,j+9} = f^{k+12}_{i+3,j+12} = 2\epsilon_{ijk},\\
&f^{1}_{i+9,j+12}{=}2\delta_{ij}, f^{2}_{i+6,j+12} = -2\delta_{ij}, f^{3}_{i+6,j+9}{=}2\delta_{ij},
\end{aligned}
\tag{21}
$$

plus the structure constants obtained from the antisymmetry relation $f^{a}_{c,b} = -f^{a}_{b,c}$. It is now straightforward, though a little tedious, to derive 16 equations fulfilled by the functions S_a, i.e.,

$$
\begin{aligned}
&\partial_t S_0 = 0,\\
&\partial_t S_1 = -2\tfrac{mc^2}{\hbar} S_2,\\
&\partial_t S_2 = -2\tfrac{c}{\hbar}(p^j - e\mathcal{A}^j) S_{j+12} + 2\tfrac{mc^2}{\hbar} S_1,\\
&\partial_t S_3 = 2\tfrac{c}{\hbar}(p^j - e\mathcal{A}^j) S_{j+9},\\
&\partial_t S_{k+3} = 2\tfrac{c}{\hbar}\epsilon_{kjl}(p^j - e\mathcal{A}^j) S_{l+6},\\
&\partial_t S_{k+6} = 2\tfrac{c}{\hbar}\epsilon_{kjl}(p^j - e\mathcal{A}^j) S_{l+3} - 2\tfrac{mc^2}{\hbar} S_{k+9},\\
&\partial_t S_{k+9} = -2\tfrac{c}{\hbar}(p^k - e\mathcal{A}^k) S_3 + 2\tfrac{mc^2}{\hbar} S_{k+6},\\
&\partial_t S_{k+12} = 2\tfrac{c}{\hbar}(p^k - e\mathcal{A}^k) S_2.
\end{aligned}
\tag{22}
$$

Note that the equations containing the 6 functions S_0, S_1, S_2, S_{13}, S_{14}, S_{15} do not couple to remaining ten equations for S_3, S_4, S_5, S_6, S_7, S_8, S_9, S_{10}, S_{11}, S_{12}. Denoting

$$
\begin{aligned}
&S_3 = h_3, \qquad && (S_4, S_5, S_6) = \boldsymbol{h}_0,\\
&(S_7, S_8, S_9) = \boldsymbol{h}_1, \qquad && (S_{10}, S_{11}, S_{12}) = \boldsymbol{h}_2,
\end{aligned}
\tag{23}
$$

we see that (22) for ten-dimensional vector $V = [h_3, \boldsymbol{h}_0, \boldsymbol{h}_1, \boldsymbol{h}_2]$ can be written in the matrix form as

$$
\partial_t V = \frac{c}{\hbar}\, M\big(\boldsymbol{p}(t)\big)\, V, \tag{24}
$$

where

$$
\boldsymbol{p}(t) = \boldsymbol{p} - e\boldsymbol{\mathcal{A}}(t), \tag{25}
$$

and the matrix M is given by (9). The same system of ordinary differential equations follows from (7) after applying the method of characteristics to first-order partial differential equations [4, 8, 10, 11]. Therefore the two vectors W and V obey the same system of ordinary differential equations. In order to identify fully V and W one needs to show that they fulfill also the same initial conditions, which for W are given by (6) and $\boldsymbol{g}^{\rm vac}_0 = 0 = \boldsymbol{g}^{\rm vac}_2$.

The Dirac wave function pertaining to the pair creation process should fulfill the Feynman boundary conditions: (i) for $t \to -\infty$ it contains only solutions of the free Dirac equation with negative energy, (ii) for $t \to \infty$ it is a combination of positive and negative energy parts with a negative energy contribution equal to the wave function of the created positron. An extensive discussion of the boundary conditions fulfilled by solutions of the Dirac equation in a classical electromagnetic field can be found in [39]. It can also be shown that the Feynman boundary conditions are "forced" by LSZ-reduction formulae for the S-matrix element of pair creation. For $t \to -\infty$, we have therefore

$$
\Phi_{\boldsymbol{p}s}(t) = \exp\left(\frac{i}{\hbar} E_{\boldsymbol{p}} t\right) w^{(-)}_{-\boldsymbol{p}s}. \tag{26}
$$

Substituting (26) into (16) with the bispinors normalized to unity, one can show that the coefficients (23) fulfill the following initial conditions for $t \to -\infty$

$$
\boldsymbol{h}^0_0 = 0 = \boldsymbol{h}^0_2, \quad h^0_3 = -\frac{2mc^2}{E_{\boldsymbol{p}}}, \quad \boldsymbol{h}^0_1 = -\frac{2c\,\boldsymbol{p}}{E_{\boldsymbol{p}}}, \tag{27}
$$

corresponding exactly to vacuum initial conditions for the vector W.

The bispinorial approach to the dynamic Sauter–Schwinger pair production by a spatially homogeneous electric field has been developed in this section. Importantly, the approach has been proven to be equivalent to the DHW formalism described in Sect. 2. And, like the DHW method, it has an advantage over other approaches. Specifically, it allows the treatment of an arbitrarily polarized time-dependent electric field. Having said that, we turn to the case of linear polarization, for which other well-established theories exist and can be tested against (see, for instance, [40, 41] and references therein).

4. Linearly polarized field and analogy with two level atom

In general, the vector W (or, equivalently V) can be expressed as a combination of ten orthonormal basis vectors $\mathbb{E}_a$

$$
W = -2\sum_{a=1}^{10} u_a \mathbb{E}_a. \tag{28}
$$

With the choice of $-\frac{1}{2}W^{\rm vac}$ as one of the basis elements, one can show that for a linearly polarized field $\boldsymbol{\mathcal{A}}(t) = \mathcal{A}(t)\boldsymbol{n}$, three vectors

$$
\mathbb{E}_1 = \frac{c}{E_{\boldsymbol{p}}\epsilon_\perp}\begin{bmatrix} -mc^2(\boldsymbol{n}\cdot\boldsymbol{p}) \\ \boldsymbol{0} \\ \dfrac{E^2_{\boldsymbol{p}}\boldsymbol{n}}{c} - c(\boldsymbol{n}\cdot\boldsymbol{p})\boldsymbol{p} \\ \boldsymbol{0} \end{bmatrix}, \quad \mathbb{E}_2 = \frac{c}{\epsilon_\perp}\begin{bmatrix} 0 \\ \boldsymbol{p}\times\boldsymbol{n} \\ \boldsymbol{0} \\ mc\,\boldsymbol{n} \end{bmatrix}, \quad \mathbb{E}_3 = \frac{1}{E_{\boldsymbol{p}}}\begin{bmatrix} mc^2 \\ \boldsymbol{0} \\ c\,\boldsymbol{p} \\ \boldsymbol{0} \end{bmatrix}, \tag{29}
$$

form a set closed under the action of $\boldsymbol{n}\cdot\nabla_{\boldsymbol{p}}$ and M in (7), where $\epsilon_\perp=\sqrt{c^2\boldsymbol{p}_\perp^2+m^2c^4}$. Note that $\mathbb{E}_3 = -\frac{1}{2}W^{\rm vac}$. Choosing $\boldsymbol{n}$ in the z-direction ($\boldsymbol{n}=\boldsymbol{e}_3$) we have

$$\frac{\partial}{\partial p_3}\mathbb{E}_1=-\frac{c\,\epsilon_\perp}{E_{\boldsymbol{p}}^2}\mathbb{E}_3,\quad \frac{\partial}{\partial p_3}\mathbb{E}_2=0,\quad \frac{\partial}{\partial p_3}\mathbb{E}_3=\frac{c\,\epsilon_\perp}{E_{\boldsymbol{p}}^2}\mathbb{E}_1,$$
$$M\mathbb{E}_1=\frac{2E_{\boldsymbol{p}}}{c}\mathbb{E}_3,\quad M\mathbb{E}_2=-\frac{2E_{\boldsymbol{p}}}{c}\mathbb{E}_1,\quad M\mathbb{E}_3=0. \tag{30}$$

Solution of (7) can be expressed as

$$W(\boldsymbol{p},t)=-2\sum_{a=1}^{3}u_a(\boldsymbol{p},t)\,\mathbb{E}_a\big(\boldsymbol{p}(t)\big). \tag{31}$$

Substituting (31) to (24) and denoting $[\ u_1,\,u_2,\,u_3\ ]=\boldsymbol{u}$, we obtain the precession-type equation for $\boldsymbol{u}$

$$\partial_t\boldsymbol{u}=\boldsymbol{a}\times\boldsymbol{u}, \tag{32}$$

with the vector $\boldsymbol{a}$ given by

$$\boldsymbol{a}=[0,\ -2\Omega_{\boldsymbol{p}}(t),\ 2\omega_{\boldsymbol{p}}(t)], \tag{33}$$

where

$$\omega_{\boldsymbol{p}}(t)=\frac{E_{\boldsymbol{p}(t)}}{\hbar}=\frac{1}{\hbar}\sqrt{c^2\boldsymbol{p}_\perp^2+c^2\big[p_3-e\mathcal{A}(t)\big]^2+m^2c^4},$$
$$\Omega_{\boldsymbol{p}}(t)=\frac{c\,e\,\epsilon_\perp\mathcal{E}(t)}{2E_{\boldsymbol{p}(t)}^2}, \tag{34}$$

and where the temporal dependence of the electric field is given by $\mathcal{E}(t)=-\dot{\mathcal{A}}(t)$. Note that the initial condition for $\boldsymbol{u}$ has the form $\boldsymbol{u}^{\rm vac}=[0,\,0,\,1]$.

Three equations resulting from (32) can be reduced to a system of two equations by expressing $\boldsymbol{u}$ in the form of a spinorial decomposition, analogous to that used in [9, 10], i.e.,

$$\boldsymbol{u}=\chi^\dagger\boldsymbol{\sigma}\chi, \tag{35}$$

where χ is the two-component spinor and $\boldsymbol{\sigma}$ are the Pauli matrices. Substitution of (35) to (32) leads to the equation for χ which has the same structure as the Schrödinger equation describing the time evolution of a two-level atom. This equation has been derived in the context of pair-creation by a different method earlier (see, e.g., [9, 40] and references therein),

$$\mathrm{i}\partial_t\begin{bmatrix}c_{\boldsymbol{p}}^{(1)}(t)\\ c_{\boldsymbol{p}}^{(2)}(t)\end{bmatrix}=\begin{bmatrix}\omega_{\boldsymbol{p}}(t) & \mathrm{i}\,\Omega_{\boldsymbol{p}}(t)\\ -\mathrm{i}\,\Omega_{\boldsymbol{p}}(t) & -\omega_{\boldsymbol{p}}(t)\end{bmatrix}\begin{bmatrix}c_{\boldsymbol{p}}^{(1)}(t)\\ c_{\boldsymbol{p}}^{(2)}(t)\end{bmatrix}, \tag{36}$$

where $c_{\boldsymbol{p}}^{(1)}(t)$ and $c_{\boldsymbol{p}}^{(2)}(t)$ are, respectively, upper and lower components of χ. Initial conditions read

$$c_{\boldsymbol{p}}^{(1)}|_{t\to-\infty}=1,\quad c_{\boldsymbol{p}}^{(2)}|_{t\to-\infty}=0. \tag{37}$$

The third component of $\boldsymbol{u}$ is equal to $|c_{\boldsymbol{p}}^{(1)}|^2-|c_{\boldsymbol{p}}^{(2)}|^2$ and for a two-level atom corresponds to "population inversion" (with opposite sign). Before the action of the electric field $u_3=1$, which corresponds to the vacuum state with no pairs. During the action of the electric field, e^+e^- pairs are created so that $|c_{\boldsymbol{p}}^{(1)}|^2<1$ and $|c_{\boldsymbol{p}}^{(2)}|^2>0$ with $|c_{\boldsymbol{p}}^{(1)}(t)|^2+|c_{\boldsymbol{p}}^{(2)}(t)|^2=1$. Hence, $|c_{\boldsymbol{p}}^{(2)}|^2$ for $t\to\infty$ can be interpreted as the momentum distribution of the created fermionic pairs, $f(\boldsymbol{p})$ (see (12)). Explicitly,

$$f(\boldsymbol{p})=1-u_3=2\big|c_{\boldsymbol{p}}^{(2)}\big|^2. \tag{38}$$

Let us note in closing this section that the system of equations similar to (38) can be derived for bosons by applying other, than those based on the Wigner formalism, methods of QED (see, e.g., [41] and references therein). However, in this case, the time-evolution is pseudounitary.

From now on, we use units where $\hbar=1$. Moreover, m and e will refer to the electron rest mass and charge, respectively.

5. Threshold effects and vortices

In our further investigations we choose an electric field $\mathcal{E}(t)$ such that

$$\mathcal{E}(t)=\begin{cases}\mathcal{E}_0\sin^4\big(\frac{1}{2N}\phi\big)\cos(\phi), & \phi\in\ [0,2\pi N],\\ 0, & \phi\notin\ [0,2\pi N],\end{cases} \tag{39}$$

where $\phi=\omega t$ and $N=3$. The integer N determines the number of cycles within the electric field pulse, and for $N\geqslant 3$ the condition

$$\int_{-\infty}^{\infty}\mathrm{d}t\,\mathcal{E}(t)=0 \tag{40}$$

is satisfied. Due to this property, the vector potential function,

$$\mathcal{A}(t)=-\int_{-\infty}^{t}\mathrm{d}\tau\ \mathcal{E}(\tau), \tag{41}$$

can be chosen such that it vanishes both in the remote past and in the far future

$$\lim_{t\to\pm\infty}\mathcal{A}(t)=0. \tag{42}$$

The shapes of both functions for $\mathcal{E}_0=0.1\mathcal{E}_S$ and $\omega=mc^2$ are presented in Fig. 1, where $\mathcal{E}_S=m^2c^3/|e|$ is the Sauter–Schwinger electric field strength [1, 3, 42]. For the electron momentum vector, we will separate its parallel and perpendicular components as measured with respect to the direction of the electric field oscillations $\boldsymbol{e}_3$ such that $\boldsymbol{p}=p_\perp\boldsymbol{e}_\perp+p_\parallel\boldsymbol{e}_3$, where $\boldsymbol{e}_\perp$ is the unit vector perpendicular to $\boldsymbol{e}_3$.

As was mentioned in Sect. 1, the process of creating electron–positron pairs in QED has many analogies with the ionization of atoms, in which the role of the time-dependent electric field is played by a strong laser pulse in the dipole approximation. In this case, the concept of photons is commonly used as quanta of energy absorbed or emitted by the system. One can then talk about multiphoton ionization and the energy threshold for that process. Moreover, such a threshold is dynamically increased as the electric field becomes stronger, which leads

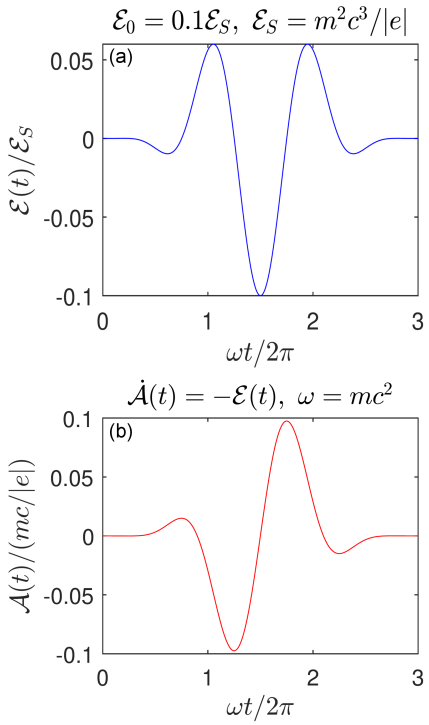

Fig. 1. (a) Time-dependent electric field strength $\mathcal{E}(t)$ for $\mathcal{E}_0 = 0.1\mathcal{E}_S$ and $N = 3$, as defined by (39), and (b) the corresponding vector potential function $\mathcal{A}(t)$. Contrary to the electric field, the amplitude of the vector potential depends on the frequency ω.

to the so-called threshold effects and channel closing in ionization [43]. It turns out that in the case of the dynamic Sauter–Schwinger process this heuristic picture can also be applied in order to describe qualitative changes in the momentum distributions of the created particles (for instance, as in the coherent energy combs studied in [40, 44]). This can be done even for the very short pulses considered here.

Another interesting effect, which appears as a result of the interaction of the time-dependent electric field with the QED vacuum, is the creation or annihilation of vortex lines in the electron momentum distributions. The properties of vortex lines and their entanglement were thoroughly analyzed in [27, 28]. In both photoionization and photodetachment, the creation and annihilation of vortex lines were studied for linearly [30] and circularly [29, 31–33] polarized fields. It was shown how the time-reversal symmetry of the laser pulse leads to the annihilation of vortex–antivortex pairs and the creation of spirals in the momentum distributions [33]. Note that such spirals have been predicted theoretically in [37] and confirmed experimentally in [38]. Moreover, the application of the DHW-function formalism allowed one to show that similar spiral structures also appear in the pair creation by a train of two circularly polarized electric field pulses of an opposite helicity [14, 15]. Therefore, the question arises: Can vortices be expected in the momentum distributions of the created pairs for linearly polarized electric field pulses?

To address this question, in Fig. 2 we present the momentum distributions of electrons created by a linearly polarized electric field pulse of different frequencies, which were selected close to the "two-photon" threshold of pair creation. For $\omega = 0.99\,mc^2$ (i.e., just before opening the "two-photon" channel), we observe two singular points for which the amplitude $c_{\boldsymbol{p}}^{(2)}$ vanishes, and the phase $\arg[c_{\boldsymbol{p}}^{(2)}]$ cannot be uniquely defined. Because of the axial symmetry of the problem, it can be concluded that these two points belong to the same vortex line. In the current case, the latter is represented by a circle in three-dimensional momentum space. In fact, one can even define the orientation of this closed line by exploiting analogies with a circuit along which an electric current flows and generates, according to Amperé's law, the vortex-type magnetic field. To this end, let us define the "magnetic field" $\boldsymbol{B}(\boldsymbol{p})$ such that

$$\boldsymbol{B}(\boldsymbol{p}) = \nabla_{\boldsymbol{p}}\Big(\arg\big[c_{\boldsymbol{p}}^{(2)}\big]\Big). \tag{43}$$

Its circulation around the singular point is $\pm 2\pi$, hence the "electric current" becomes $I = \pm 2\pi$ if we put the magnetic permeability $\mu_0 = 1$. In particular, for $\omega = 0.99\,mc^2$ (Fig. 2a), we have '$-$' for $(p_\parallel = 0, p_\perp > 0)$ and the current flows behind the plane, whereas for $(p_\parallel = 0, p_\perp < 0)$ we have '$+$' and the current flows towards the reader. Thus the orientation of the vortex line can be uniquely attributed to the direction of the "electric current". As the frequency ω increases, we observe the appearance of a new vortex line. The case of $\omega = mc^2$ (which is the threshold frequency for the two-photon pair creation) corresponds to a transition in which, for $\boldsymbol{p} = \boldsymbol{0}$, the radius of the new vortex circle is close to zero (Fig. 2b and e). After exceeding this value (the case of $\omega = 1.01\,mc^2$ in Fig. 2c and f), the second circular vortex line appears, with an orientation opposite to the previous one (panels (d–f)). While increasing the frequency ω, the radii of both circular vortex lines also grow. This, in turn, results in the merging of the two well-defined lobes of high probability into a single structure, the maximum of which is found at zero momentum. This situation is discussed in Sect. 6.

In Fig. 3 we demonstrate the same phenomenon, but for a larger amplitude of the electric field. The only significant difference is that now the threshold frequency for the two-photon pair creation is shifted upwards and its value is between $1.1\,mc^2$ (one vortex line) and $1.2\,mc^2$ (two vortex lines). A plausible interpretation of this fact can be based on analogies with multiphoton ionization, in which, for a larger intensity of the electromagnetic field, the so-called ponderomotive shift of the threshold energy is observed [43]. Similar effects, but in the context of photodetachment by circularly polarized laser pulses, were discussed in [32].

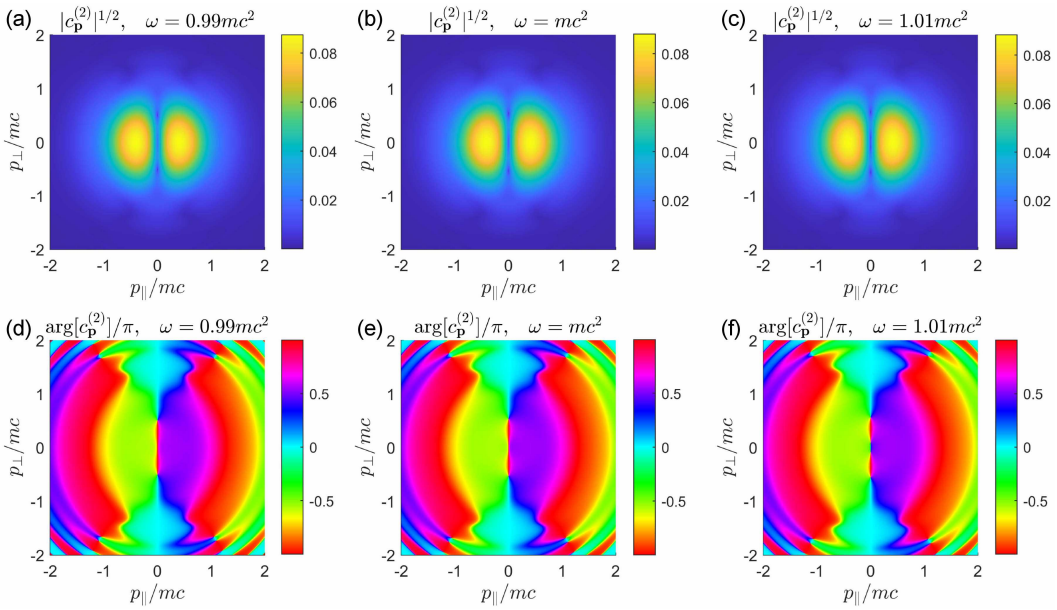

Fig. 2. Momentum distributions of electrons created from the QED vacuum by the electric field illustrated in Fig. 1. In panels (a–c), the distributions $|c_{\boldsymbol{p}}^{(2)}|^{1/2}$ (the power 1/2 is chosen for visual purposes) are presented for three chosen frequencies ω (equivalent to photon energies). In panels (d–f), the corresponding phases of $c_{\boldsymbol{p}}^{(2)}$ are demonstrated.

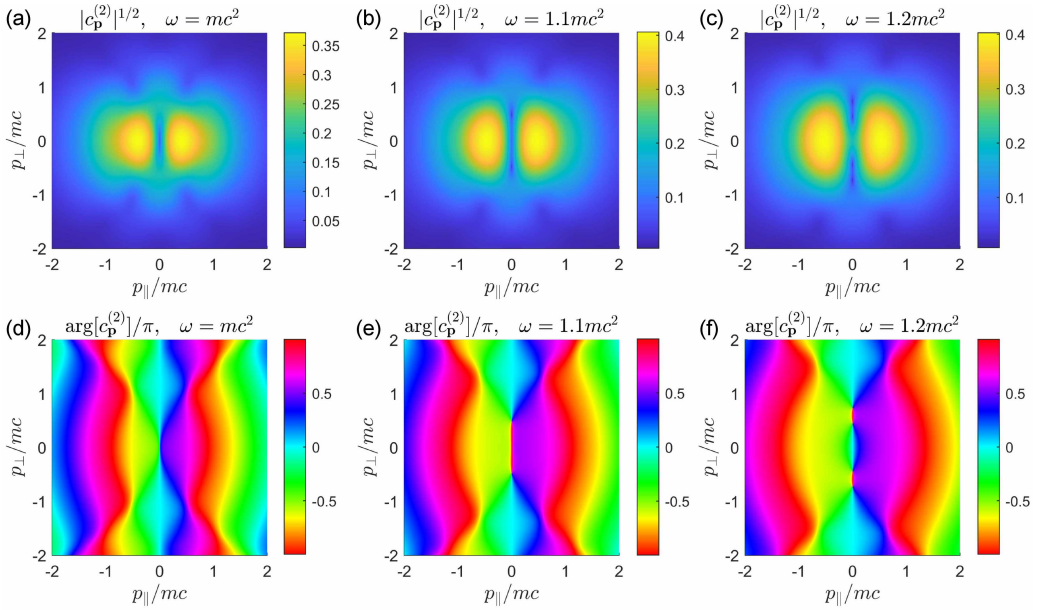

Fig. 3. The same description as in Fig. 2, but for larger electric field amplitude $\mathcal{E}_0 = 0.5\mathcal{E}_S$ and larger frequencies.

6. Longitudinal and transverse momentum sharing

The Schwinger formula for the probability rate of pair production per unit volume in the case of a constant (or slowly-changing-in-time) electric field can be derived using the tunneling formalism [45]. According to this formula, an increment of the perpendicular momentum of the particles, $|\boldsymbol{p}_\perp|$, is accompanied by a rapidly vanishing creation rate. However, for rapidly changing fields, tunneling theory is no longer applicable. This is supported by the analysis presented above because the momentum distributions for pair production are not elongated in the direction of the electric field. As it has been shown in [36], for sufficiently high frequencies ω, particles prefer to be created in the direction perpendicular to the electric field. This counterintuitive

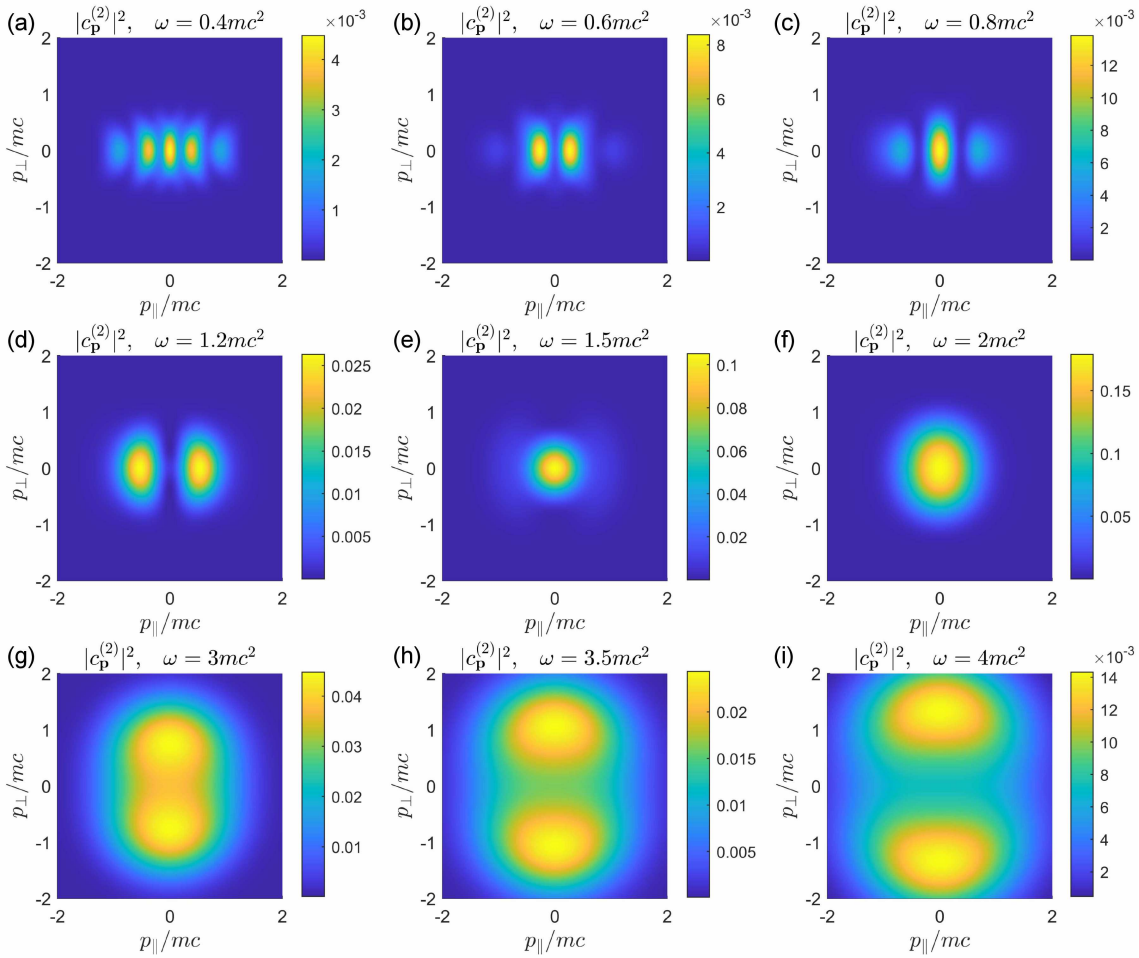

Fig. 4. Momentum distributions of electrons created by an oscillating electric field for different frequencies and for electric field amplitude $\mathcal{E}_0 = 0.5\mathcal{E}_S$. Starting from the one-photon threshold frequency, at roughly $\omega = 2\,mc^2$, a qualitative change in the shapes of high-probability structures is observed.

phenomenon is illustrated in Fig. 4. For low frequencies $\omega \leq 0.8\,mc^2$, the distributions are concentrated around the axis of vanishing transverse momentum. However, as the frequency increases, the distributions begin to concentrate around zero momentum. This happens until the one-photon threshold is reached. A further increase of frequency causes the position of the high-probability regions in the distribution to migrate towards the direction perpendicular to the electric field (i.e., towards larger $p_\perp$). Furthermore, at $\omega = 4\,mc^2$, the high-probability zone in the three-dimensional space takes the shape of a torus centered around $\boldsymbol{p}_\perp = \mathbf{0}$. This means that under such conditions the particles prefer to be ejected in the direction perpendicular to the electric field vector. As shown in [36], the distribution for pair creation, when integrated over particles momenta, starts to saturate (or even decreases) with increasing frequency, leading to the seemingly unexpected stabilization phenomenon. In fact, the stabilization effects appear to be quite common in the strong-field QED, as discussed for instance in [46–50].

In summary, although we have concentrated our discussion on the fermionic distribution function $f(\boldsymbol{p})$ and the phase of the momentum amplitude $c_{\boldsymbol{p}}^{(2)}$, the other components of the DHW-functions (8) can be also determined by applying (35), (31) and (29). This topic is, however, beyond the scope of the present work and is going to be considered in due course.

7. Conclusions

In this paper, we formulated the bispinorial approach to the production of e^-e^+ pair in spatially homogeneous electric fields. The method turned out to be equivalent to the DHW formalism, which was introduced in [4]. We have shown that the production of Sauter–Schwinger pair with linearly polarized time-dependent electric field is formally reduced to solving a two-level model, in compliance with [40] (see also references therein). The advantage of this approach is that one gains access to the probability amplitudes and, therefore, to their

phases. The latter allows to uniquely identify vortices and antivortices in the momentum distributions of created pairs. As it has been demonstrated in our paper, for a linearly polarized pulsed electric field, they appear in pairs. We also analyzed the vortex patterns while increasing the field frequency across a two-photon threshold. While we have observed a new vortex–antivortex pair, the general features of the momentum distributions also change across the threshold. Specifically, we have seen that below the one-photon threshold, particles are created most efficiently along the polarization direction of the electric field, whereas above the threshold — in the perpendicular direction. This shows the different characteristics of the Sauter–Schwinger process while passing from low- to high-frequency regimes of electric-field–vacuum interactions.

Acknowledgments

The work of (F.C.V., K.K., and J.Z.K.) was supported by the National Science Centre (Poland) under Grant No. 2018/31/B/ST2/01251.

References

[1] F. Sauter, *Z. Phys.* **69**, 742 (1931).

[2] W. Heisenberg, H. Euler, *Z. Phys.* **98**, 714 (1936).

[3] J.S. Schwinger, *Phys. Rev.* **82**, 664 (1951).

[4] I. Białynicki-Birula, P. Górnicki, J. Rafelski, *Phys. Rev. D* **44**, 1825 (1991).

[5] G.R. Shin, I. Białynicki-Birula, J. Rafelski, *Phys. Rev. A* **46**, 645 (1992).

[6] I. Białynicki-Birula, E.D. Davis, J. Rafelski, *Phys. Lett. B* **311**, 329 (1993).

[7] Ł. Rudnicki, Ph.D. Thesis., Center for Theoretical Physics, PAS, 2021.

[8] F. Hebenstreit, R. Alkofer, and H. Gies, *Phys. Rev. D* **82**, 105026 (2010).

[9] I. Białynicki-Birula, Ł. Rudnicki, *Phys. Rev. D* **83**, 065020 (2011).

[10] I. Białynicki-Birula, Ł. Rudnicki, A. Wienczek, arXiv:1108.2615v3, 2013.

[11] A. Blinne, H. Gies, *Phys. Rev. D* **89**, 085001 (2014).

[12] C. Kohlfürst, Ph.D. Thesis, arXiv:1512.06082, 2015.

[13] A. Blinne, E. Strobel, *Phys. Rev. D* **93**, 025014 (2016).

[14] Z.L. Li, Y.J. Li, B.S. Xie, *Phys. Rev. D* **96**, 076010 (2017).

[15] Z.L. Li, B.S. Xie, Y.J. Li, *J. Phys. B* **52**, 025601 (2019).

[16] I. Białynicki-Birula, Z. Białynicka-Birula, *Phys. Rev. A* **104**, 022203 (2021).

[17] X. Sheng, R. Fang, Q. Wang, D.H. Rischke, *Phys. Rev. D* **99**, 056004 (2019).

[18] F. Hebenstreit, R. Alkofer, H. Gies, *Phys. Rev. Lett.* **107**, 180403 (2011).

[19] D. Berényi, S. Varró, V.V. Skokov, P. Lévai, *Phys. Lett. B* **749**, 210 (2015).

[20] H. Al-Naseri, J. Zamanian, G. Brodin, *Phys. Rev. E* **104**, 015207 (2021).

[21] M. Mohamedsedik, L.-J. Li, B.S. Xie, *Phys. Rev. D* **104**, 016009 (2021).

[22] C. Kohlfürst, R. Alkofer, *Phys. Lett. B* **756**, 371 (2016).

[23] C. Kohlfürst, *Eur. Phys. J. Plus* **133**, 191 (2018).

[24] C. Kohlfürst, *Phys. Rev. D* **101**, 096003 (2020).

[25] G. Brodin,J. Zamanian, *Rev. Mod. Plasma Phys.* **6**, 4 (2022).

[26] I. Białynicki-Birula, M. Cieplak, J. Kamiński, *Theory of Quanta*, Oxford University Press, New York 1992.

[27] I. Białynicki-Birula, Z. Białynicka-Birula, C. Śliwa, *Phys. Rev. A* **61**, 032110 (2000).

[28] A.J. Taylor, *Analysis of Quantised Vortex Tangle*, Springer, Cham 2017.

[29] L. Geng, F. Cajiao Vélez, J.Z. Kamiński, L.-Y. Peng, K. Krajewska, *Phys. Rev. A* **102**, 043117 (2020).

[30] F. Cajiao Vélez, L. Geng, J.Z. Kamiński, L.-Y. Peng, K. Krajewska, *Phys. Rev. A* **102**, 043102 (2020).

[31] L. Geng, F. Cajiao Vélez, J.Z. Kamiński, L.-Y. Peng, K. Krajewska, *Phys. Rev. A* **104**, 033111 (2021).

[32] F. Cajiao Vélez, *Phys. Rev. A* **104**, 043116 (2021).

[33] M.M. Majczak, F. Cajiao Vélez, J.Z. Kamiński, K. Krajewska, *Opt. Express* **30**, 43330 (2022).

[34] I. Białynicki-Birula, Z. Białynicka-Birula, *Phys. Rev. Lett.* **118**, 114801 (2017).

[35] I. Białynicki-Birula, Z. Białynicka-Birula, *Phys. Rev. A* **100**, 012108 (2019).

[36] K. Krajewska, J.Z. Kamiński, *Phys. Rev. A* **100**, 012104 (2019).

[37] J.M.N. Djiokap, S.X. Hu, L.B. Madsen, N.L. Manakov, A.V. Meremianin, A.F. Starace, *Phys. Rev. Lett.* **115**, 113004 (2015).

[38] D. Pengel, S. Kerbstadt, D. Johannmeyer, L. Englert, T. Bayer, M. Wollenhaupt, *Phys. Rev. Lett.* **118**, 053003 (2017).

[39] I. Białynicki-Birula, Z. Białynicka-Birula, *Quantum Electrodynamics*, Ch. 5, Pergamon Press Ltd., Polish Scientific Publishers 1975.

[40] J.Z. Kamiński, M. Twardy, K. Krajewska, *Phys. Rev. D* **98**, 056009 (2018).

[41] K. Krajewska, J.Z. Kamiński, *Phys. Rev. A* **100**, 062116 (2019).

[42] F. Sauter, *Z. Phys.* **73**, 547 (1932).

[43] K. Krajewska, I.I. Fabrikant, A.F. Starace, *Phys. Rev. A* **74**, 053407 (2006).

[44] E. Akkermans, G.V. Dunne, *Phys. Rev. Lett.* **108**, 030401 (2012).

[45] L. Labun, J. Rafelski, *Phys. Rev. D* **79**, 057901 (2009).

[46] J.Z. Kamiński, K. Krajewska, F. Ehlotzky, *Phys. Rev. A* **74**, 033402 (2006).

[47] L. Labun, J. Rafelski, *Phys. Rev. D* **98**, 016006 (2018).

[48] S. Evans, J. Rafelski, *Eur. Phys. J. A* **57**, 341 (2021).

[49] A.I. Titov, U. Hernandez Acosta, B. Kämpfer, *Phys. Rev. A* **104**, 062811 (2021).

[50] U. Hernandez Acosta, A.I. Titov, B. Kämpfer, *New J. Phys.* **23**, 095008 (2021).